Geomechanics and Engineering, *Vol. 27, No. 3 (2021) 253-262*
https://doi.org/10.12989/gae.2021.27.3.253

Impact of curing time on UCS-electrical resistivity relation of cement grouted sands

Hyunwook Choo[1a], Woojin Lee[2b] and Changho Lee*[3]

[1]*Department of Civil and Environmental Engineering, Hanyang University, Seoul 04763, Republic of Korea*
[2]*School of Civil, Environmental and Architectural Engineering, Korea University, Seoul 02841, Republic of Korea*
[3]*Department of Civil Engineering, Chonnam National University, Gwangju 61184, Republic of Korea*

(Received March 9, 2021, Revised August 27, 2021, Accepted October 8, 2021)

Abstract. As the curing process proceeds, both the strength and electrical resistivity (ρ_{mix}) of cement-based (or cement-grouted) materials increase, leading to the nondestructive ρ_{mix} measurement technique is very appealing in the assessment/monitoring of the quality of cement-grouted materials. However, the strength gain of cement-grouted sands with time differs from the increase in ρ_{mix} with time. Thus, the relationship between unconfined compressive strength (UCS) and ρ_{mix} can be affected by the curing time. This study evaluated the effect of curing time on the relationship between ρ_{mix} and UCS of sands grouted with microcement. The ultimate goal of this study is to estimate UCS over time of cement-grouted sands based on ρ_{mix}. Three silica sands with different median particle sizes were grouted with microcement at different water-to-cement ratios (wc) of 1.0, 1.5, and 2.0. Both unconfined compression test and electrical resistivity measurement test were conducted. Results demonstrate that curing time, particle size, and wc influenced both ρ_{mix} and UCS of tested grouted sands in a similar manner; therefore, a direct relationship between ρ_{mix} and UCS can be established. However, the complex impact of curing time on the relation between UCS and ρ_{mix} and the nonlinear increase in UCS with time hinder the capture of adequate interplay between UCS, ρ_{mix}, and curing time. Because a nonlinear increase in UCS with time can be represented by hyperbolic model, an estimation method for hyperbolic model parameters is newly suggested in this study based on ρ_{mix} at early curing days.

Keywords: curing time; electrical resistivity; hyperbolic mode; microcement; unconfined compressive strength

1. Introduction

Since a permeation grouting is a method of injecting cementitious materials into the void space of sandy soils to improve various engineering properties (Han 2015, Nonveiller 2013, Park and Oh 2018), it has been adopted as one of the key ground improvement methods in the field of geotechnical or geological engineering (Park and Oh 2018). The assessment of the reinforcement degree for soft ground grouted with cementitious materials is mostly based on measurement of the unconfined compressive strength (UCS) of a grouted specimen (Consoli *et al*. 2015). However, 1) an unconfined compression test is time consuming and expensive to prepare specimens; and 2) the sampling process could disturb the specimen to be used for the unconfined compression test (Avci and Mollamahmutoğlu 2016, Dano *et al*. 2004, Markou and Droudakis 2013, Sunitsakul *et al*. 2012). Therefore, nondestructive testing methods including elastic and electromagnetic wave measurements, ultrasound, and electrical measurements, have been recently used to evaluate/monitor the quality of grouted ground because these methods are economical. In addition, they allow continuous real-time measurements (Santarato *et al*. 2011, Taylor and Arulanandan 1974, Xu *et al*. 2018, Zhang *et al*. 2014, Zhang *et al*. 2012). Among them, an electrical resistivity measurement is very appealing for assessing or monitoring the quality of cement-based (or cement-grouted) materials.

Several previous studies have tried to established a direct relationship between electrical resistivity (ρ_{mix}) and UCS (Ferreira and Jalali 2010, Lim *et al*. 2017, Liu *et al*. 2008, Vincent *et al*. 2017, Zhang *et al*. 2012) because similar factors, such as sand particle size, relative density, and water-to-cement ratio (wc) can influence both ρ_{mix} and UCS. However, most of these previous studies did not consider a curing time effect on the relationship between ρ_{mix} and UCS despite the fundamental distinction in the mechanism between the development of ρ_{mix} and UCS with the time (Wei *et al*. 2012, Zhang *et al*. 2012). Because UCS is determined by the quality of cementation bonding between soil particles, UCS nonlinearly increases with time due to a hydration process (Yoon *et al*. 2020). In contrast, ρ_{mix} is determined by the connectivity of pore space (Choo *et al*. 2019). Because the formation of a hydration product can clog the pore space at a relatively earlier curing period, the time-dependency of ρ_{mix} is different from that of UCS.

Consequently, this study investigated the impact of curing time on the relationship between ρ_{mix} and UCS of microcement grouted sands. A microcement has been extensively employed as a grout material because of its

*Corresponding author, Associate Professor
E-mail: changho@jnu.ac.kr
[a]Associate Professor
E-mail: choohw@hanyang.ac.kr
[b] Professor
E-mail: woojin@korea.ac.kr

ISSN: 2005-307X (Print), 2092-6219 (Online)

higher injectability than Ordinary Portland cement. In addition, it is safer for the environment than a chemical grout (Lee *et al*. 2019, Mollamahmutoglu and Yilmaz 2011, Pantazopoulos *et al*. 2012). Grouted sand specimens were prepared at different water-to-cement ratios (1.0, 1.5, and 2.0). Unconfined compression test and electrical resistivity measurement test were then performed. Differences in UCS and ρ_{mix} according to the curing time were determined, and the relationship between UCS and ρ_{mix} was then investigated. Furthermore, a new method for estimating the UCS for cement grouted sands based on ρ_{mix} at an early curing time was suggested in this study.

2. Electrical resistivity of cement-based materials

The measured electrical conductivity (σ_{mix}) of various geomaterials can be expressed as a function of the total of particle conduction K_p (i.e., electronic conduction through contacts between solid particles), pore water conduction K_w (i.e., ionic conduction via the pore water), and surface conduction K_s (i.e., special form of ionic conduction via the diffuse double layer) (Choo and Burns 2014). Because mobile ions in cement grains can be dissolved during a hydration reaction, resulting in an increase in pore water conductivity σ_w, it is presumed that measured electrical conductivity of cement-based (or cement-grouted) sands (σ_{mix}) can be stated as the sum of K_w and K_p (i.e., $K_w >> K_s$). Since K_p values of both cement grains and sand particles are extremely low, σ_{mix} is mainly determined by K_w as (Komine 1997, Liu *et al*. 2008):

$$\sigma_{mix} = K_w = \sigma_w \cdot \frac{n}{T^2} \quad (1)$$

where n is the porosity and T is the tortuosity. The reciprocal of σ_{mix} is electrical resistivity (ρ_{mix}), and when the power function between tortuosity and porosity (i.e., $T = n^{-p}$, where p is a fitting parameter) is assumed, Eq. (1) becomes Eq. (2) as (Choo and Burns 2014):

$$\rho_{mix} = \rho_w \cdot \frac{T^2}{n} = \rho_w \cdot n^{-2p-1} \quad (2)$$

where ρ_w is pore water resistivity ($\rho_w = 1/\sigma_w$). Note that Eq. (2) is equivalent to the original Archie's equation under fully saturated conditions. Therefore, by employing the saturation factor of Archie (1942), Eq. (2) becomes Eq. (3) as (Cardoso and Dias 2017):

$$\rho_{mix} = \rho_w \cdot \frac{T^2}{n} \cdot S^m \quad (3)$$

where S is the degree of saturation and m is the fitting parameter. Because T, n, and S determine the connectivity of pore water space, Eq. (3) highlights that the measured ρ_{mix} of cement-grouted materials is mainly determined by ρ_w and the connectivity of pore water space (Xiao and Li 2009).

3. Experimental programs

3.1 Materials and testing specimen preparation

In this study, three uniform angular silica sands with median particle sizes (D_{50}) ranging from 0.33 mm to 0.87 mm were used (Fig. 1). Basic material properties of tested sands are shown in Table 1. The microcement produced by Ssangyong Co.(Korea) was selected in this study. Chemical composition and physical properties of the microcement, provided by manufacturer, are shown in Table 2.

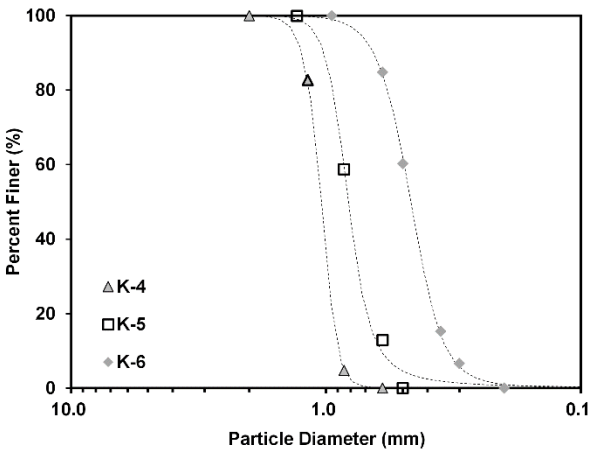

Fig. 1 Grain size distribution curves of tested sands

Table 1 Index Properties of Tested Sands

Type	G_s	D_{50} (mm)	C_u	e_{max}	e_{min}
K-4	2.65	1.01	1.19	1.08	0.71
K-5	2.65	0.81	1.47	1.07	0.69
K-6	2.65	0.47	1.52	1.04	0.66

Note: G_s = specific gravity; D_{50} = median particle size; C_u = uniformity coefficient; e_{max} = maximum void ratio; and e_{min} = minimum void ratio.

Table 2 Chemical Composition and Physical Properties of Microcement

Chemical composition	SiO_2	Al_2O_3	CaO	Fe_2O_3	K_2O	MgO	SO_3	Na_2O
	27.5	11.2	51.3	1.7	0.44	4.8	2.1	0.17
Physical properties	G_s	D_{max}	S_a	UCS (MPa) at wc = 0.52				
				1 day	7 day	28 day		
	3.03	< 15 μm	> 860 m^2/kg	10.3	28.9	57.6		

Note: G_s = specific gravity; D_{max} = maximum particle size; S_a = specific surface.

Water-to-cement ratios (wc) of 1.0, 1.5 and 2.0 were selected to prepare grout suspensions because the microcement used in this study with wc smaller than 1 showed as high viscosity (> 0.01 Pa· s) and the microcement with wc greater than 2 showed high bleeding (> 15%). Fig. 2 shows the sample preparation equipment used in this study (Avci and Mollamahmutoğlu 2016, Dano *et al*. 2004). Predetermined amount of the microcement was mechanically blended with a deionized water to have wc of 1.0, 1.5, and 2.0. Then 3% bentonite (Duksan, Korea) by weight of the microcement was added into the cement suspension to reduce bleeding. The sand specimens were constructed in a split plastic mold with a relative density of

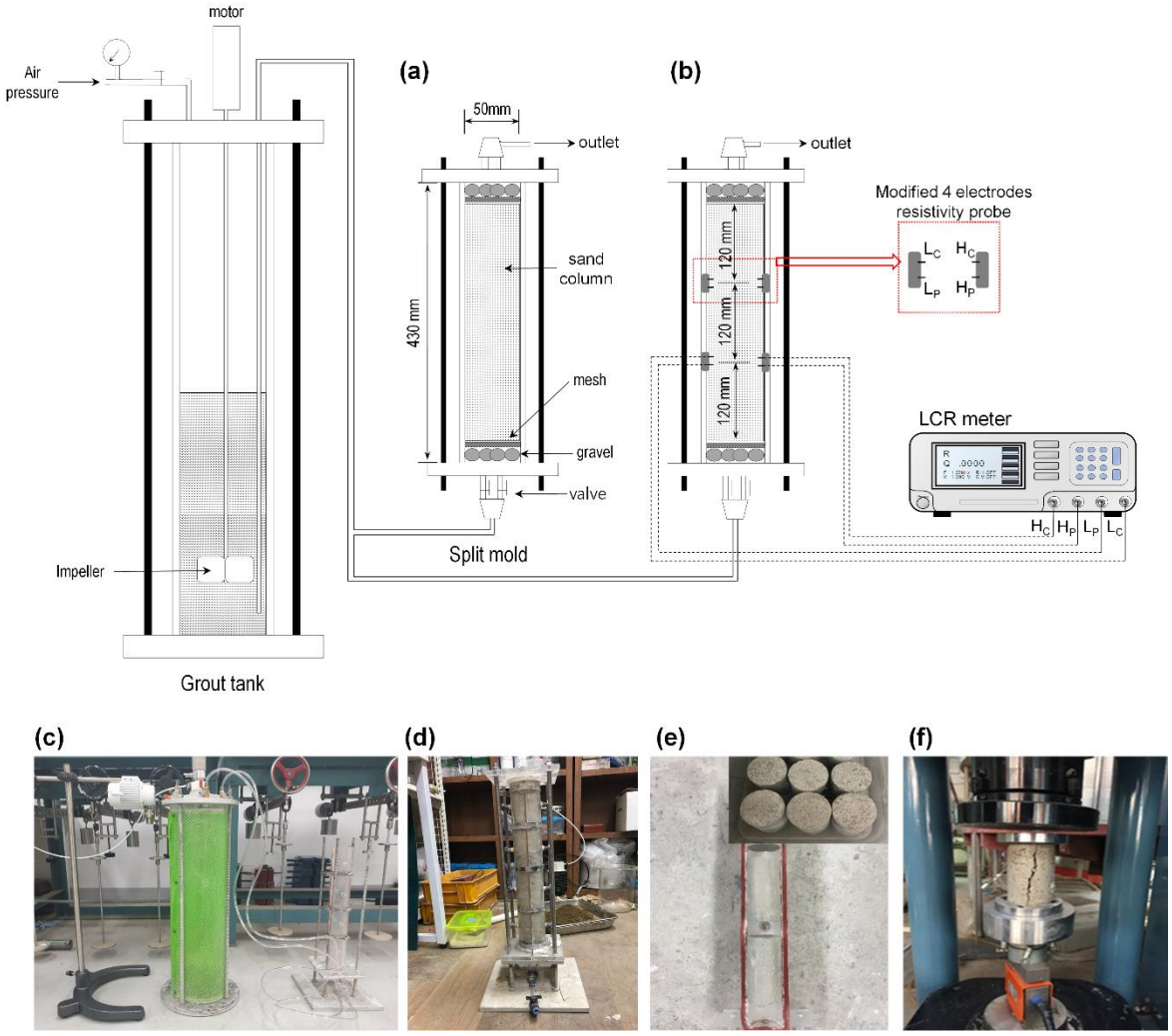

Fig. 2 Schematic drawing and pictures of the device for testing specimen preparation and test setup: (a) unmodified split mold for the unconfined compression test; (b) modified split mold equipped with an electrode resistivity probe; (c) grout tank and split mold; (d) grouted specimen after the completion of injection; (d) trimmed specimens; and (e) unconfined compression test. Note: electrode = stainless steel; H_C = high current; H_P = high potential; L_C = low current; and L_P = low potential

~70% using a water pluviation method. Grout suspensions were injected from the bottom of the split plastic mold by an air pressure (Fig. 2). When the injected volume of the grout suspension reached two times the void volume of the sand specimen, the injection was finished. Note that the maximum injection pressure applied in this study was less than 700 kPa to minimize the fabric change in the granular skeleton. Detailed description of the sample preparation process can be found in studies of Lee *et al*. (2019) and Yoon *et al*. (2020).

After the cement suspension was injected, these grouted specimens were rested in a sealed container with a relative humidity of ~ 99% and a constant temperature of ~ 23°C. For the unconfined compression test, specimens were extruded from the split mold after 3, 7, 14, and 28 days of curing and cut to a height of 100 mm (Fig. 2). Note that the inside of the split mold was covered by a lubricant for easy separation of specimens from the mold. In contrast, electrical resistivity was measured without a demolding process.

3.2 Testing methods

The unconfined compression test was conducted at a loading rate of 1 mm/min to measure unconfined compressive strength (UCS) of each grouted specimen. To apply a uniform stress, an unbonded cap was covered at the top and bottom of the cylindrical specimen with a diameter of 50 mm and a height of 100 mm. UCS was measured after different curing time (i.e., 3, 7, 14 and 28 days). Note that average UCS value of three replicate tests is reported as the representative UCS value of each specimen at a given testing condition. Individual variation was smaller than 10% of the average value.

A modified four electrodes system was adopted to evaluate the reliable electrical resistivity of grouted sands without electrochemical effects (i.e., ion accumulation on the electrode), as shown in Fig. 2 (Won *et al*. 2019). An LCR meter (Keysight E4980A) was used to measure the electrical current flowing between the two current electrodes and the electrical resistance between the two

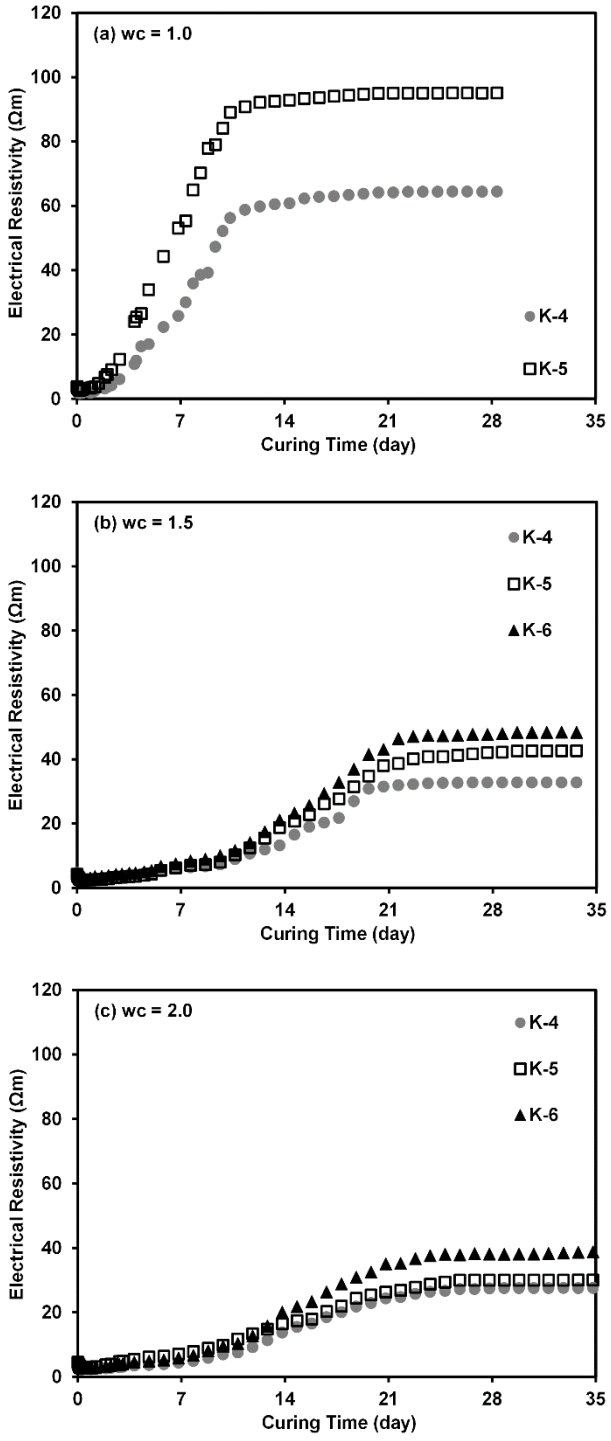

Fig. 3 Changes in electrical resistivity of tested materials as a function of curing time: (a) wc = 1.0; (b) wc = 1.5; (c) wc = 2.0. Reported values are the average of three tests with the coefficient of variation < 8.8%, and the electrical resistivity measurements were carried out for 28-35 days to confirm the asymptotic electrical resistivity values under the tested conditions..

potential electrodes. The operating frequency was chosen to be 10 kHz to prevent electrode polarization and electrical resonance. Based on the predetermined calibration factor, measured electrical resistance was changed to resistivity.

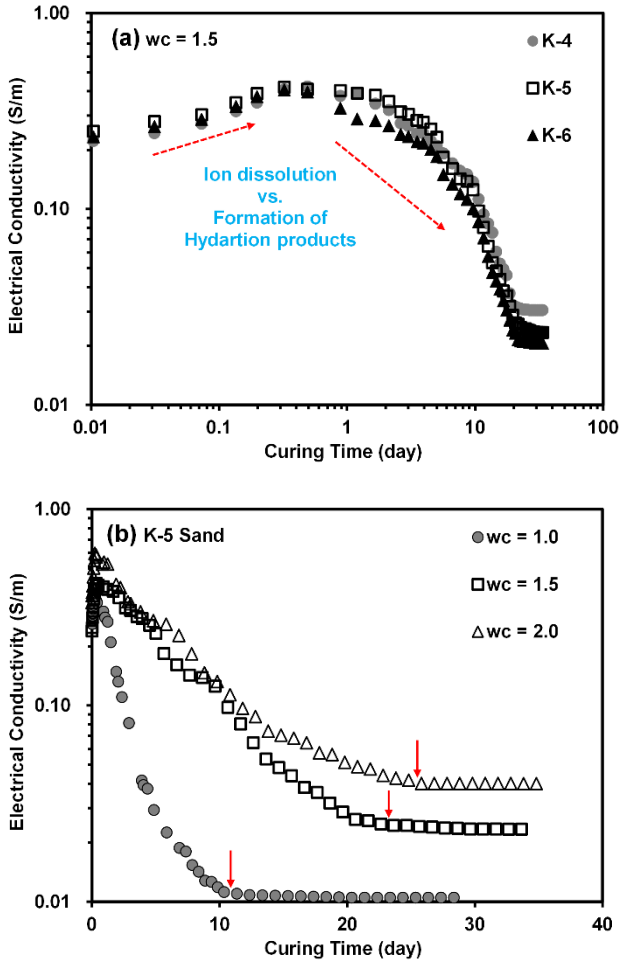

Fig. 4 Changes in electrical conductivity of tested materials according to curing time: (a) three sands at wc = 1.5; and (b) K-5 sand at three different wc ratios

4. Results and discussion

4.1 Electrical resistivity / Electrical conductivity

Fig. 3 displays changes in electrical resistivity (ρ_{mix}) of all tested grouted sands with different water-to-cement ratios (wc) according to the curing time. Measured results for K-6 sand with a wc of 1.0, implying the smallest particle (or pore) size and the greatest viscosity, were excluded from Fig. 3 because of filtration (Markou and Droudakis 2013). The cement hydration process consumes free water, which is a carrier for the transport of ions, to form hydration products, indicating a decrease in degree of saturation (S). In addition, a decrease in porosity (n) and an increase in tortuosity (T) will occur during a hydration process because cement hydration products can rapidly fill the available water-filled pore space. Therefore, measured ρ_{mix} values of all tested materials generally increased with increasing curing time. Fig. 3 also shows that the measured ρ_{mix} at a given wc increased with decreasing sand particle size because of a greater specific surface. Note that with an increase in specific surface, cement grains can effectively coat the surface of sand particles, resulting in a more tortuous conduction path for pore water conduction.

Additionally, the measured ρ_{mix} increased with a decrease in wc. Since wc directly determines the volume fraction of a hydration product (Sun *et al*. 2005, Taylor and Arulanandan 1974, Voigt *et al*. 2005), the connectivity for pore water conduction will decrease with a decrease in wc.

The change in ρ_{mix} at an early curing period was very different from that at a later curing period (Fig. 3): (1) at first, ρ_{mix} showed a very slight decrease with curing time (< 1 day of curing); (2) there was a minimal increase in ρ_{mix} with curing time (< 3-10 days of curing); (3) ρ_{mix} increased dramatically with curing time, reaching an almost steady value after 12-24 days of curing. To clarify the evolution of electrical properties of grouted sands at an early curing period, the change of electrical conductivity ($\sigma_{mix} = 1/\rho_{mix}$) was also plotted with curing time in logarithmic scale. As shown in Fig. 4, measured σ_{mix} at the initial curing period increased with curing time because mobile ions including Na^+, K^+, SO_4-, $Al(OH)_4$-, and Ca^{2+} can be melted out from cement pastes, resulting in a decrease in pore water resistivity (Eq. (3)) (Wei and Li 2005, Xiao and Li 2009). However, the formation of hydration products such as ettringite and calcium silicate hydrate gel (C-S-H) can lead to a gradual break of connectivity of the pore water space, consequently increasing the electrical resistivity with a further increase in curing time. As a result, because of the offset mechanism between a decrease in pore water resistivity and a gradual break of pore water connectivity, ρ_{mix} very slowly increased (or σ_{mix} very slowly decreases) with time at an early curing period (< 3-10 days of curing) (Figs. 2 and 3) (Wei and Li 2005, Xiao and Li 2009). As hydration further proceeded, the available water-filled pore space, which was the main path for pore water conduction, was rapidly filled by hydration products without showing more decrease in pore water resistivity. Therefore, σ_{mix} rapidly decreased (or ρ_{mix} rapidly increased) with time. Finally, when the path for pore water conduction was discontinued because of the hydration products, an almost constant σ_{mix} (or ρ_{mix}) was observed (Figs. 2 and 3).

The time required to obtain the almost constant σ_{mix} (or ρ_{mix}) for K-5 sand indicated by arrows in Fig. 4(b) was affected by wc. In addition, the time when ρ_{mix} started to increase rapidly with time, which might represent the starting time of solidification, was affected by wc (Figs. 3(a)-3(c)) (Li *et al*. 2007). A smaller wc indicates a greater fraction of cement grains at a given pore space. Because each cement grains can individually react with water (Van Breugel 1993, Ye *et al*. 2003), the consumption of free water can be accelerated with decreasing wc (Sariosseiri and Muhunthan 2009). Furthermore, previous studies have reported a quicker formation of connected hydration products with decreasing wc (Sun *et al*. 2005, Voigt *et al*. 2005), resulting in a quicker disconnection of the pore water conduction path. Therefore, with a decrease in wc, the starting time when ρ_{mix} rapidly increased with time decreased, and the time required to have an almost constant ρ_{mix} values decreased.

4.2 Unconfined compressive strength

Fig. 5 displays variations of unconfined compressive strength (UCS) of all tested grouted sands according to curing time. As shown in Fig. 5, UCS increased with increasing curing time because of the time-dependent hardening of hydration products formed at contacts between sand particles (Abbasi and Mahdieh 2018, Cardoso *et al*. 2017, Consoli *et al*. 2011, Sun *et al*. 2005). Similar results have been reported in previous studies (Choo *et al*. 2018,

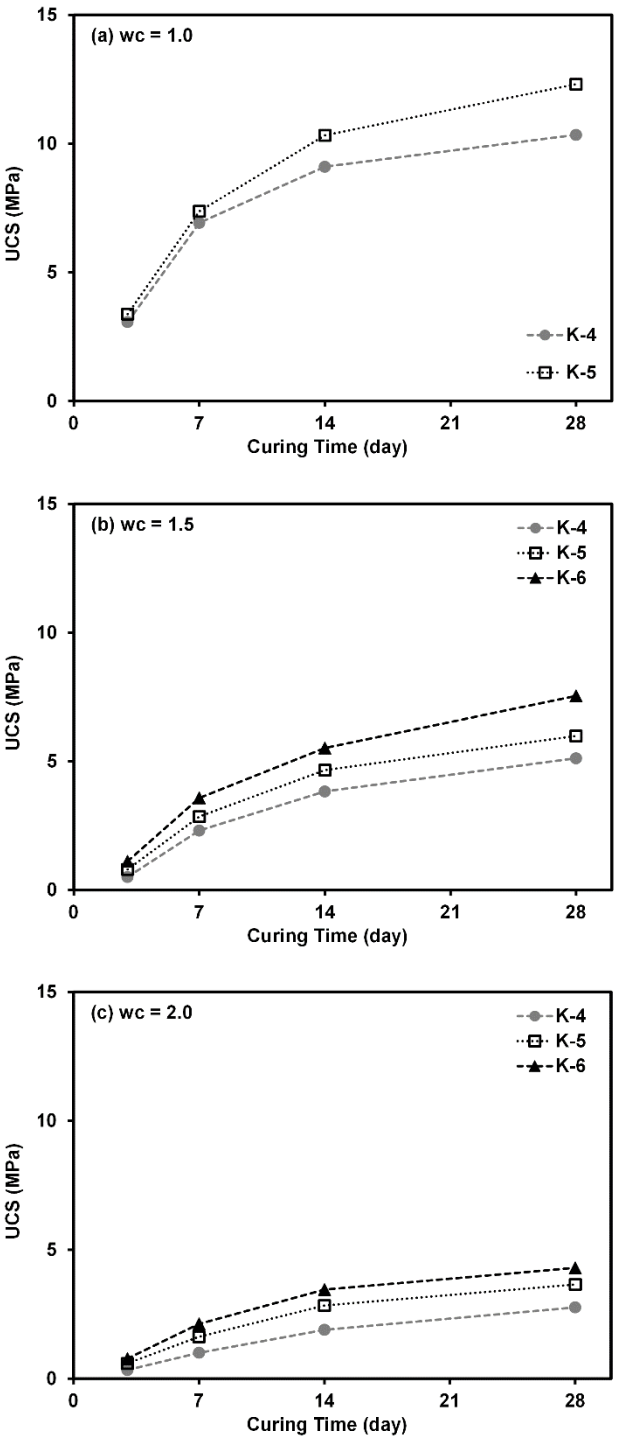

Fig. 5 Changes in unconfined compressive strength (UCS) of tested materials as a function of curing time: (a) wc = 1.0; (b) wc = 1.5; (c) wc = 2.0. Reported values are the average of three tests with the coefficient of variation < 7.6%.

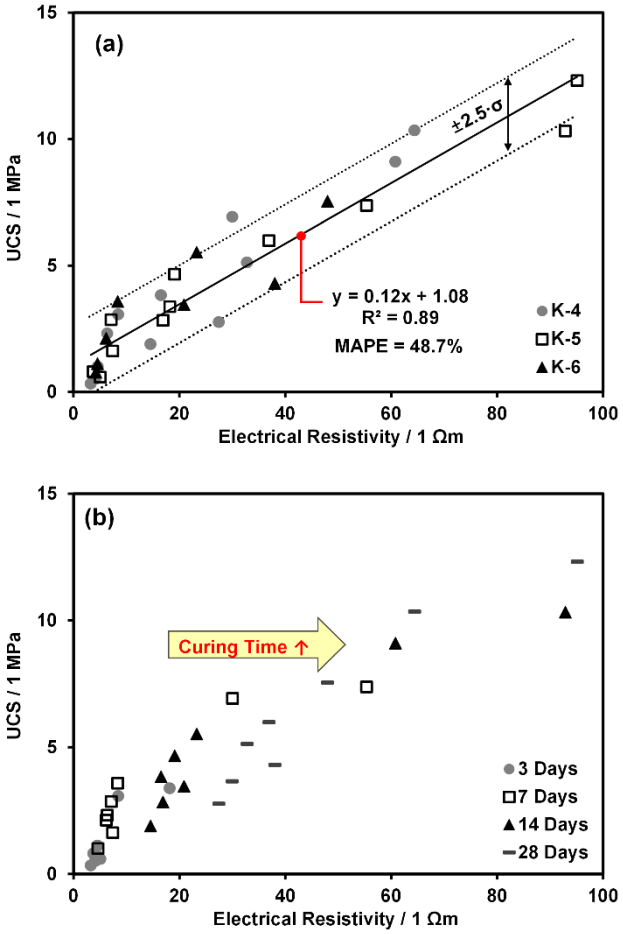

Fig. 6 Relationship between the ρ_{mix} and UCS of tested three grouted sands: (a) data legend = sand type (sand particle size); and (b) data legend = curing days. σ = standard deviation

Choo *et al*. 2017, Markou and Droudakis 2013). Fig. 5 showed that the measured UCS increased with decreasing median particle size of sand because of an increase in specific surface to which cement particles could adsorb (Yoon *et al*. 2020). In addition, UCS increased with decreasing wc because of an increase in the strength of cementation contact bonds (Lee *et al*. 2019).

Comparison between Figs. 3 and 5 demonstrated that the same variables (i.e., curing time, sand particle size, and wc) affected both ρ_{mix} and UCS in a similar manner: 1) both ρ_{mix} and UCS increased with increasing curing time; 2) both ρ_{mix} and UCS increased with decreasing sand particle size; and 3) both ρ_{mix} and UCS increased with decreasing wc. This analogy between ρ_{mix} and UCS implies that it might be possible to develop a direct relationship between ρ_{mix} and UCS. However, the comparison between Figs. 3 and 5 also clearly demonstrated that the time-dependencies of ρ_{mix} and UCS were very different: ρ_{mix} values were almost constant at a relatively early curing time (after 12-24 days of curing), whereas the time required for the relatively constant UCS was not measurable under the tested curing time. Therefore, the following sections aimed to develop a direct relationship between ρ_{mix} and UCS and evaluate the effect of curing time on the relationship between ρ_{mix} and UCS.

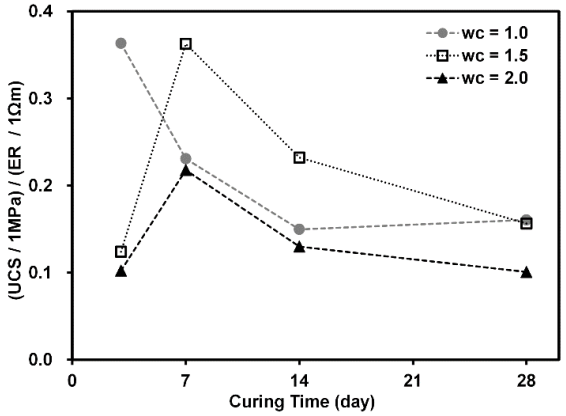

Fig. 7 Effect of curing time on the ratio between UCS and electrical resistivity (ER) at three different wc for K-4 sand. Note the results for K-5 and K-6 sands are comparable with the above figure

4.3 Relationship between ρ_{mix} and UCS

Since similar parameters such as curing time, particle size, and wc controlled both ρ_{mix} and UCS of tested grouted sands, a direct relationship between ρ_{mix} and UCS could be established as shown in Fig. 6. Consistent with results of previous studies (Ferreira and Jalali 2010, Lim *et al*. 2017, Liu *et al*. 2008, Zhang *et al*. 2012), Fig. 6(a) shows that the relationship between ρ_{mix} and UCS of three grouted sands can be expressed as a single linear function, reflecting that the relationship between ρ_{mix} and UCS is independent of sand particle size:

$$\frac{\text{UCS}}{1\text{MPa}} = 0.12 \cdot \frac{\rho_{mix}}{1\Omega m} + 1.08 \quad (4)$$

Although the coefficient of determination is relatively high (R^2 = 0.89), Fig. 6(a) also indicates that UCS values at a given ρ_{mix} show very wide variations (±2.5·standard deviation). Therefore, the mean absolute percentage error (MAPE) is calculated to identify the difference between the measured UCS and the estimated UCS based on Eq. (4).

$$\text{MAPE} = \frac{1}{M}\sum_{i=1}^{M}\left|\frac{measured\ \ value - estimated\ \ value}{measured\ \ value}\right| \quad (5)$$

where M is the number of data points. The calculated MAPE is around 48.7%, indicating that Eq. (4) yields a poor agreement between the measured and estimated UCS values.

4.4 Effects of curing time on the relationship between UCS and ρ_{mix}

To figure out the effect of time on the relationship between ρ_{mix} and UCS, four different curing time were selected as data legend instead of sand type as shown in Fig. 6(b). The relationship between ρ_{mix} and UCS generally shifted to the right with increasing curing time, indicating greater UCS values at a given ρ_{mix} with decreasing curing time. However, in the case where the measured ρ_{mix} was

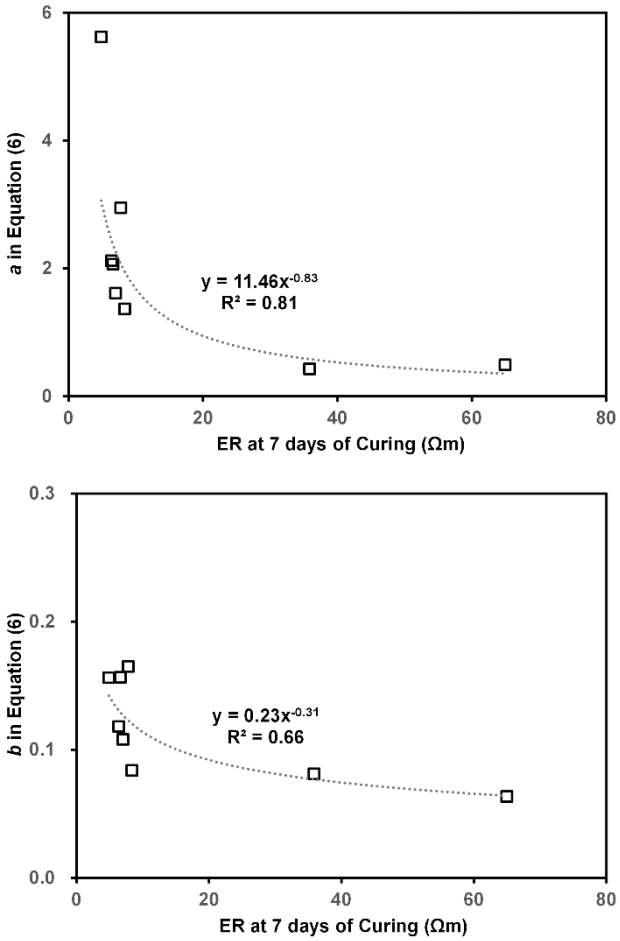

Fig. 8 Variations of hyperbolic parameters *a* and *b* in Equation (6) as a function of electrical resistivity (ER) at 7 days of curing

greater than 50 Ωm (i.e., grouted sands with wc of 1.0 at later curing days), an inverse trend between ρ_{mix} and UCS was also observed, reflecting the complex impact of time on the relation between ρ_{mix} and UCS. Results of quantitative evaluation of the impact of curing time will be shown in the next paragraph. Consequently, the estimated UCS based on ρ_{mix} could be significantly different from the measured UCS with increasing curing time due to different time-dependencies of ρ_{mix} and UCS. Note that the linear relationship between ρ_{mix} and UCS revealed that both were mainly affected by the formation of hydration products (Ferreira and Jalali 2010). However, the difference in time-dependency reflects the fundamental difference between the strength gain and the increase in electrical resistivity of cement-grouted sand as hydration proceeds (Zhang *et al*. 2012).

The ratio of UCS to ρ_{mix} as function of curing time is plotted in Fig. 7. It can be observed in Fig. 7 that the ratio of UCS to ρ_{mix} was affected by curing time and wc. The formation of hydration products can be briefly described as follows (Berodier and Scrivener 2015, Bishnoi and Scrivener 2009, Mindess *et al*. 2003, Scrivener *et al*. 2015, Yoon *et al*. 2020):

1) At an early curing stage, loose hydration products are formed to rapidly fill in the empty pore space. The filling of water-filled pore spaces with loose hydration products might be enough to disconnect the path for the transport of ions (i.e., pore water conduction), leading to an almost constant ρ_{mix} at relatively earlier curing ages (< 12 -24 days of curing) (Fig. 3).

2) The available pore space for the growth of hydration products will decrease, resulting in densification of hydration products. The formation of dense inner products gives additional cementation bonding strength to cement-grouted sands. Thus, when UCS nonlinearly increases with time, it takes more time to obtain an almost constant UCS value. Note that under the tested curing time, asymptotic UCS values were not observed (Fig. 5). Consequently, the ratio of UCS to ρ_{mix} generally decreased with an increase in curing time (Figs. 6 and 7).

3) The hydration process ceases when the growth of hydration products terminates due to limited pore space.

When wc was 1.5 or 2.0, the ratio of UCS to ρ_{mix} increased with time at an early curing period (< 7 days) (Fig. 7). As mentioned earlier, because of the offset mechanism between the decrease in pore water resistivity and a gradual break of pore water connectivity, ρ_{mix} very slowly increased with time at an early curing period, especially for grouted sands with wc of 1.5 or 2.0 (Fig. 3(b) and 3(c)). Therefore, the increasing rate of ρ_{mix} relative to time at an early curing period was smaller than that of UCS. When wc of 1.0, the ratio of UCS to ρ_{mix} very slightly increased with time after 14 days of curing. Because the ρ_{mix} of grouted sand with wc of 1.0 showed a negligible change after 14 days of curing (Fig. 3(a)), the increasing rate of ρ_{mix} relative to time at a later curing period was smaller than that of UCS.

Figs. 6 and 7 clearly indicate that the impact of curing time should be included in the relationship between UCS and ρ_{mix} of tested grouted sands. However, the complex impact of curing time (i.e., increasing and then decreasing with time or decreasing and then slightly increasing with time) on the ratio between UCS and ρ_{mix} hinders the capture of the adequate interplay between UCS, ρ_{mix}, and curing time.

4.5 Estimating time-dependent UCS using ρ_{mix} at the curing age of 7 days

The nonlinear strength gain of cement-based materials with curing time (t) can be best represented by the hyperbolic model as (Carino 1984, Yoon *et al*. 2020):

$$UCS = UCS_{ult} \times \frac{kt}{1+kt} = \frac{t}{\frac{1}{k \times UCS_{ult}} + \frac{t}{UCS_{ult}}} = \frac{t}{a+bt} \quad (6)$$

where UCS_{ult} is the ultimate (or long-term) unconfined compressive strength; k is the factor indicating the initial slope between UCS and curing time; a is the reciprocal of $k \cdot UCS_{ult}$; and b is the reciprocal of ultimate UCS. From the measured UCS values with time, the hyperbolic model parameters a and b in Eq. (6) can be easily determined (see details in Yoon *et al*. 2020). Yoon *et al*. (2020) have shown that both UCS_{ult} and k in Eq. (6) increase with decreasing

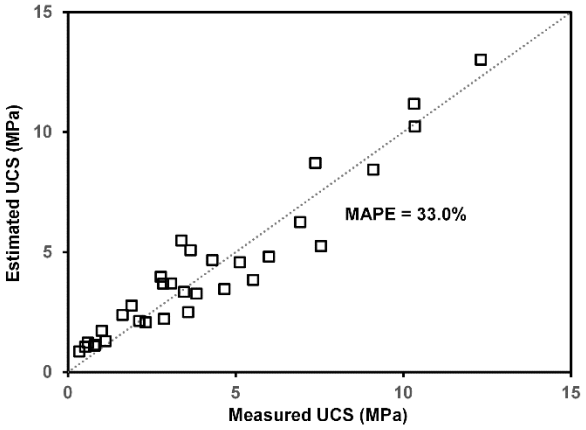

Fig. 9 Comparison between the measured UCS and estimated UCS using Equation (6)

wc and sand particle size. Because the electrical resistivity of tested materials is also mainly determined by wc and sand particle size, it can be postulated that parameters *a* and *b* in Eq. (6) are associated with ρ_{mix}, similar to the direct relation between UCS and ρ_{mix} (Fig. 6).

Fig. 8 shows variations of *a* and *b* in Eq. (6) as a function of ρ_{mix} at 7 days of curing. Note that rapid determination of long-term or ultimate UCS, which is an input parameter for the design strength of cement-stabilized soils, based on the electrical resistivity measurement at early curing period is very promising because it permits an economical design of soil stabilization (Ferreira and Jalali 2010,Wei *et al*. 2012). Previous studies have shown possible relations between ρ_{mix} at early curing period and UCS at 28 days of curing. In contrast, this study aimed to estimate hyperbolic model parameters in Eq. (6). Thus, the prediction of both long-term UCS and UCS over time is possible based on ρ_{mix} at an early curing period. Because *a* and *b* parameters, which reflect the ultimate UCS, are associated with ρ_{mix} at an early curing period, R-squared values are not very high (> 0.66) (Fig. 8). However, Fig. 8 clearly demonstrated that both *a* and *b* parameters decreased with increasing ρ_{mix} at 7 days of curing.

Fig. 9 shows comparison between measured UCS and estimated UCS using Eq. (6) with input of *a* and *b* parameters based on Fig. 8. To quantify the difference between the measured and the estimated UCS, MAPE value was calculated (Eq. (5)). It was found to be 33.0%, indicating more reasonable prediction of UCS of tested cement grouted sands compared to Eq. (4). This enhanced prediction of UCS of tested grouted sands is very remarkable because the prediction of UCS based on Eq. (6) is only based on ρ_{mix} at an early curing period whereas Eq. (4) or Fig. 6(a) is developed based on the one-to-one match between UCS and ρ_{mix} over time.

6. Summary and conclusions

The relationship between electrical resistivity (ρ_{mix}) and unconfined compressive strength (UCS) of three sands grouted with microcement was investigated in this study. This study particularly evaluated the effect of curing time on the relationship between ρ_{mix} and UCS. Although we found that there was an acceptable linear relationship between UCS and ρ_{mix} in general based on the same influencing variables on both ρ_{mix} and UCS of tested materials, consistent with previous studies, the estimation of UCS based on ρ_{mix} should be made by considering the curing time because of the difference in time-dependency. Due to the complex impact of curing time on the relation between ρ_{mix} and UCS and the nonlinear increase in UCS with time, a UCS estimating method was newly suggested in this study. The suggested UCS estimating formula was based on the hyperbolic model. Thus, both long-term UCS and UCS time could be adequately estimated based on ρ_{mix} at an early curing time. Finally, this study clearly shows that an almost constant ρ_{mix} value does not guarantee the termination of hydration process. Thus, caution is required when using the electrical resistivity measurement technique to monitor cement hydration process with consequent evaluation of the degree of ground improvement.

Acknowledgments

This work is supported by a Korea Agency for Infrastructure Technology Advancement (KAIA) grant funded by the Ministry of Land, Infrastructure and Transport (Grant 21SCIP-C151438-03).

Conflict of interest statement

On behalf of all authors, the corresponding author states that there is no conflict of interest relevant.

References

Abbasi, N. and Mahdieh, M. (2018), "Improvement of geotechnical properties of silty sand soils using natural pozzolan and lime", *Int. J. Geo-Eng.*, **9**(1), 1-12. https://doi.org/10.1186/s40703-018-0072-4.

Archie, G.E. (1942), "The electrical resistivity log as an aid in determining some reservoir characteristics", *Transactions American Institute Mining Metallurgical Engineers*, **146**, 54-61. https://doi.org/10.2118/942054-G.

Avci, E. and Mollamahmutoğlu, M. (2016), "UCS roperties of superfine cement–grouted sand", *J. Mater. Civil Eng.*, **28**(12), 06016015. https://doi.org/10.1061/(ASCE)MT.1943-5533.0001659.

Berodier, E. and Scrivener, K. (2015), "Evolution of pore structure in blended systems", *Cement Concrete Res.*, **73**, 25-35. https://doi.org/10.1016/j.cemconres.2015.02.025.

Bishnoi, S. and Scrivener, K.L. (2009), "Studying nucleation and growth kinetics of alite hydration using μic", *Cement Concrete Res.*, **39**(10), 849-860. https://doi.org/10.1016/j.cemconres.2009.07.004.

Cardoso, R. and Dias, A.S. (2017), "Study of the electrical resistivity of compacted kaolin based on water potential", *Eng. Geology*, **226**, 1-11. https://doi.org/10.1016/j.enggeo.2017.04.007.

Cardoso, R., Ribeiro, D. and Néri, R. (2017), "Bonding effect on the evolution with curing time of compressive and tensile strength of sand-cement mixtures", *Soils Foundations*, **57**(4), 655-668. https://doi.org/10.1016/j.sandf.2017.04.006.

Carino, N.J. (1984), "The maturity method: Theory and application", *Cement Concrete Aggregates*, **6**(2), 61-73.

https://doi.org/10.1520/CCA10358J.

Choo, H. and Burns, S.E. (2014), "Review of Archie's equation through theoretical derivation and experimental study on uncoated and hematite coated soils", *J. Appl. Geophys.*, **105**, 225-234. https://doi.org/10.1016/j.jappgeo.2014.03.024.

Choo, H., Lee, W. and Lee, C. (2018), "Overconsolidation and cementation in sands: Impacts on geotechnical properties and evaluation using dilatometer tests", *Geotech. Testing J.*, **41**(5), 915-929. https://doi.org/10.1520/GTJ20170368.

Choo, H., Nam, H. and Lee, W. (2017), "A practical method for estimating maximum shear modulus of cemented sands using unconfined compressive strength", *J. Appl. Geophys.*, **147**, 102-108. https://doi.org/10.1016/j.jappgeo.2017.10.012.

Choo, H., Nam, H., Lee, C., Lee, W. and Burns, S. (2019), "Monitoring hydration process and quality of sand grouted with microfine-cement using shear wave velocity and electrical conductivity measurements", *Proceedings of E3S Web of Conferences*, EDP Sciences, 11012. https://doi.org/10.1051/e3sconf/20199211012.

Consoli, N.C., Cruz, R.C. and Floss, M.F. (2011), "Variables controlling strength of artificially cemented sand: influence of curing time", *J. Mater. Civil Eng.*, **23**(5), 692-696. https://doi.org/10.1061/(ASCE)MT.1943-5533.0000205.

Consoli, N.C., Winter, D., Rilho, A.S., Festugato, L. and Teixeira, B.D. (2015), "A testing procedure for predicting strength in artificially cemented soft soils", *Eng. Geology*, **195**, 327-334. https://doi.org/10.1016/j.enggeo.2015.06.005.

Dano, C., Hicher, P.-Y. and Tailliez, S. (2004), "Engineering properties of grouted sands", *J. Geotech. Geoenviron. Eng.*, **130**(3), 328-338. https://doi.org/10.1061/(ASCE)1090-0241(2004)130:3(328),

Ferreira, R. M. and Jalali, S. (2010), "NDT measurements for the prediction of 28-day compressive strength", *NDT E Int.*, **43**(2), 55-61. https://doi.org/10.1016/j.ndteint.2009.09.003.

Han, J. (2015), *Principles and Practice of Ground Improvement*, John Wiley and Sons, NJ, USA.

Komine, H. (1997), "Evaluation of chemical grouted soil by electrical resistivity", *Proceedings of the Institution of Civil Engineers-Ground Improvement*, **1**(2), 101-113. https://doi.org/10.1680/gi.1997.010203.

Lee, C., Nam, H., Lee, W., Choo, H. and Ku, T. (2019), "Estimating UCS of cement-grouted sand using characteristics of sand and UCS of pure grout", *Geomech Eng*, **19**(4), 343-352. https://doi.org/10.12989/gae.2019.19.4.343.

Li, Z.J., Xiao, L.Z. and Wei, X.S. (2007), "Determination of concrete setting time using electrical resistivity measurement", *J. Mater. Civil Eng.*, **19**(5), 423-427. https://doi.org/10.1061/(Asce)0899-1561(2007)19:5(423),

Lim, S., Lee, W., Choo, H. and Lee, C. (2017), "Utilization of high carbon fly ash and copper slag in electrically conductive controlled low strength material", *Construct. Build. Mater.*, **157**, 42-50. https://doi.org/10.1016/j.conbuildmat.2017.09.071.

Liu, S.Y., Du, Y.J., Han, L.H. and Gu, M.F. (2008), "Experimental study on the electrical resistivity of soil-cement admixtures", *Environ Geol*, **54**(6), 1227-1233. https://doi.org/10.1007/s00254-007-0905-5.

Markou, I. and Droudakis, A. (2013), "Factors affecting engineering properties of microfine cement grouted sands", *Geotech. Geologic. Eng.*, **31**(4), 1041-1058. https://doi.org/10.1007/s10706-013-9631-9.

Mindess, S., Young, F. and Darwin, D. (2003), *Concrete 2nd Edition*, Prentice Hall, NJ, USA.

Mollamahmutoglu, M. and Yilmaz, Y. (2011), "Engineering properties of medium-to-fine sands injected with microfine cement grout", *Marine Georesourc. Geotechnol.*, **29**(2), 95-109. https://doi.org/10.1080/1064119X.2010.517715.

Nonveiller, E. (2013), *Grouting Theory and Practice*, Elsevier, Amsterdam, Netherlands.

Pantazopoulos, I., Markou, I., Christodoulou, D., Droudakis, A., Atmatzidis, D., Antiohos, S. and Chaniotakis, E. (2012), "Development of microfine cement grouts by pulverizing ordinary cements", *Cement Concrete Compos.*, **34**(5), 593-603. https://doi.org/10.1080/1064119X.2010.517715.

Park, D. and Oh, J. (2018), "Permeation grouting for remediation of dam cores", *Eng. Geology*, **233**, 63-75. https://doi.org/10.1016/j.enggeo.2017.12.011.

Santarato, G., Ranieri, G., Occhi, M., Morelli, G., Fischanger, F. and Gualerzi, D. (2011), "Three-dimensional Electrical Resistivity Tomography to control the injection of expanding resins for the treatment and stabilization of foundation soils", *Eng. Geology*, **119**(1-2), 18-30. https://doi.org/10.1016/j.enggeo.2011.01.009.

Sariosseiri, F. and Muhunthan, B. (2009), "Effect of cement treatment on geotechnical properties of some Washington State soils", *Eng. Geology*, **104**(1-2), 119-125. https://doi.org/10.1016/j.enggeo.2008.09.003.

Scrivener, K. L., Juilland, P. and Monteiro, P. J. (2015), "Advances in understanding hydration of Portland cement", *Cement Concrete Res.*, **78**, 38-56. https://doi.org/10.1016/j.cemconres.2015.05.025.

Sun, Z., Ye, G. and Shah, S. P. (2005), "Microstructure and early-age properties of Portland cement paste–effects of connectivity of solid phases", *ACI Mater. J.*, **102**(2), 122-129.

Sunitsakul, J., Sawatparnich, A. and Sawangsuriya, A. (2012), "Prediction of unconfined compressive strength of soil–cement at 7 days", *Geotech. Geologic. Eng.*, **30**(1), 263-268. https://doi.org/10.1007/s10706-011-9460-7.

Taylor, M. A. and Arulanandan, K. (1974), "Relationships between electrical and physical properties of cement pastes", *Cement Concrete Res.*, **4**(6), 881-897. https://doi.org/10.1016/0008-8846(74)90023-4.

Van Breugel, K. (1993), "Simulation of hydration and formation of structure in hardening cement-based materials", Ph.D. Dissertation, Delft University of Technnology, Netherlands.

Vincent, N. A., Shivashankar, R., Lokesh, K. and Jacob, J. M. (2017), "Laboratory electrical resistivity studies on cement stabilized soil", *Int. Scholarly Res. Notices*, **2017**. https://doi.org/10.1155/2017/8970153.

Voigt, T., Ye, G., Sun, Z. H., Shah, S. P. and van Breugel, K. (2005), "Early age microstructure of Portland cement mortar investigated by ultrasonic shear waves and numerical simulation", *Cement Concrete Res.*, **35**(5), 858-866. https://doi.org/10.1016/j.cemconres.2004.09.004.

Wei, X. and Li, Z. (2005), "Study on hydration of Portland cement with fly ash using electrical measurement", *Mater Struct*, **38**(277), 411-417. https://doi.org/10.1617/14108.

Wei, X.S., Xiao, L.Z. and Li, Z.J. (2012), "Prediction of standard compressive strength of cement by the electrical resistivity measurement", *Construct. Build. Mater.*, **31**, 341-346. https://doi.org/10.1016/j.conbuildmat.2011.12.111.

Won, J., Park, J., Choo, H. and Burns, S. (2019), "Estimation of saturated hydraulic conductivity of coarse-grained soils using particle shape and electrical resistivity", *J. Appl. Geophys.*, **167**, 19-25. https://doi.org/10.1016/j.jappgeo.2019.05.013.

Xiao, L. Z. and Li, Z. J. (2009), "New Understanding of Cement Hydration Mechanism through Electrical Resistivity Measurement and Microstructure Investigations", *J. Mater. Civil Eng.*, **21**(8), 368-373. https://doi.org/10.1061/(Asce)0899-1561(2009)21:8(368),

Xu, W., Tian, X. and Cao, P. (2018), "Assessment of hydration process and mechanical properties of cemented paste backfill by electrical resistivity measurement", *Nondestructive Testing Evaluation*, **33**(2), 198-212. https://doi.org/10.1080/10589759.2017.1353983.

Ye, G., Van Breugel, K. and Fraaij, A. (2003), "Three-dimensional microstructure analysis of numerically simulated cementitious materials", *Cement Concrete Res.*, **33**(2), 215-222. https://doi.org/10.1016/S0008-8846(02)00889-X.

Yoon, B., Lee, W., Lee, C. and Choo, H. (2020), "Time-Dependent Variations of Compressive Strength and Small-Strain Stiffness of Sands Grouted with Microfine Cement", *J. Geotech. Geoenviron. Eng.*, **146**(4), 06020001. https://doi.org/10.1061/(ASCE)GT.1943-5606.0002207.

Zhang, D. W., Cao, Z.G., Fan, L.B., Liu, S.Y. and Liu, W.Z. (2014), "Evaluation of the influence of salt concentration on cement stabilized clay by electrical resistivity measurement method", *Eng. Geology*, **170**, 80-88. https://doi.org/10.1016/j.enggeo.2013.12.010.

Zhang, D.W., Chen, L. and Liu, S.Y. (2012), "Key parameters controlling electrical resistivity and strength of cement treated soils", *J Cent South Univ*, **19**(10), 2991-2998. https://doi.org/10.1007/s11771-012-1368-8.

GC